Calibration of LISS-3 sensor on-board Resourcesat-2A using integrated approach

Yogdeep Desai[a*], Neeraj Badal[b], Pratibha Soni[b], B Kartikeyan[d]

a Scientist "SF",IAQD/SIPG/Space Applications Centre-Ahmedabad
b Scientist "SC",IAQD/SIPG/Space Applications Centre-Ahmedabad
c Scientist "H",IAQD/SIPG/Space Applications Centre-Ahmedabad

*Corresponding author: yogdeepdesai@sac.isro.gov.in

Abstract

Pre and Post launch calibration is an important activity to ensure radiometric fidelity of sensor throughout the life of the mission. The pre-launch laboratory calibration, also called Light Transfer Characteristics, establishes uniformity in the response among the detector elements to a similar incident radiation. It also associates the input intensity to the sensor's response. However, the exercise is performed only on limited discrete levels and there is an uncertainty in dark signal characterization. The deep dark space surrounding moon image can be used for characterizing dark noise but although moon has a temporally stable radiometry, it is composed of wide range of intensities from the surface Mare and highlands. This article discusses an integrated approach of calibrating the LISS3 sensor on-board Resourcetsa-2A wherein Laboratory, Moon as well as Cross Comparison with contemporary sensor has been utilized for radiometric calibration. The calibration coefficients have been validated using target spectral signature, Lunar data and Radiometric calibration site.

Introduction

The remote sensing sensors represent the earth surface in terms of its geometric and radiometric characteristics. The degree of closeness, with which the radiometry is recorded depends on the accuracy and consistency of sensor's radiometric calibration over the lifetime of the mission. Every sensor is calibrated in the laboratory during pre-launch stage for its response to input energy. However, due to thrust during launch, harsh climate of space and aging of components the pre-launch calibration requires monitoring and thus post-launch calibration is carried out periodically to maintain the radiometric precision.

Various methods are used for the post-launch calibration including on-board calibration sources and solar diffusers (Ron Morfitt , Julia Barsi , Raviv Levy , Brian Markham , Esad Micijevic ,Lawrence Ong , Pat Scaramuzza and Kelly Vanderwerff, 2015). In absence of such provision, earth surfaces with suitable characteristics are used for post-launch calibration of sensors (Teillet P M, 2006). Post-launch calibration is also carried out with reference to another sensor (Teillet P M, 2006) which is assumed to be calibrated independently. This method of cross calibration has its own suitability conditions. Moon has also been used as a stable radiometric source (Desai, Bhavsar, & Kartikeyan, 2011), with no intervening atmosphere between the sensor and the source (the moon).

Each of the aforementioned approaches have their own strengths and limitations. An integrated calibration approach has been employed in the radiometric calibration and validation of Resourcesat-2A (R2A) mission having three-tier imaging capability with coarser resolution AWiFS (R2AAW), medium resolution LiSS3 (R2AL3) and high resolution Liss4 (R2AL4) sensors. This note discusses the

approach and the result of calibration of R2AL3 carried out during the commissioning phase of R2A mission.

Radiometric calibration methodologies

The approach of radiometric calibration varies with the stage at which the calibration is carried out e.g. pre-launch calibration uses standard source, capable of generating varying amount of known radiance, under controlled environmental conditions in laboratory. This section discusses different approaches used during pre-launch and post-launch stage for the radiometric calibration of sensor.

Pre-launch radiometric calibration

The pre-launch radiometric calibration of remote sensing system, also called Light Transfer Characteristics (LTC) exercise (RESOURCESAT-2 DQE Team, 2010), is a combination of a) normalizing the difference between inter-element response to same input radiance: **P**hoto **R**esponse **N**on-**U**niformity (PRNU) and b) establishing relationship between known input radiance and system's normalized response to this radiance in the form of counts.

The output of LTC exercise is a set of gain and bias coefficients per detector element which when applied to the measured count, results in the same output for same input energy. The input intensity is selected in such a way so as to cover the dynamic range of the sensor being calibrated. The characterization of sensor is thus carried out during LTC exercise for limited number of intensity levels which can be generated in the laboratory. Further *the zero-intensity level, which is required for quantifying the inherent sensor noise when, measured in laboratory has an added component of background radiation creating uncertainty in the reliability of its assessment. It can also lead to a pseudo-linear characterization of sensor's response.*

Post-launch radiometric calibration

The continuation of radiometric quality during the life time of the sensor requires post-launch monitoring and re-calibration of sensors. Use of natural and artificial (IAQD Calval Team, 2017) sites with specific characteristics and lunar acquisition are methods used by many teams. Cross calibration between a calibrated sensor and the target sensor using simultaneous imaging of calibration sites has also been used. Cross calibration has also been found to be resource-effective method.

Figure 1 Lunar surface showing radiometrically varying surface

Moon disc is found to have stable radiometric property and a spectral profile similar to that of earth's features (Stone & Kieffer, 2007). The deep space surrounding the moon image allows characterization of sensor's response to dark background. However, the moon has always been considered in the form of disc-integrated source because the lunar surface consists of widely varying radiometric range [Figure 1] and hence considered for monitoring radiometric stability over time and validation.

Resourcesat-2A mission

The Resourcesat-2A (R2A) was launched on 7Dec2016 as a continuity mission of Resourcesat2 (RS2) with three sensors on board viz. Low resolution AWiFS, mediums resolution LISS3 and high resolution LISS4. The specifications of R2A LISS3 sensor are given in Table 1.

Table 1 R2A LISS3 Sensor Specifications

Sensor	Central Wavelength /Bandwidth (nm)	Saturation Radiance (mW/cm2/um/sr)	Quantization (bits)	Output Spatial resolution (m)	Swath (km)
LISS3 (R2AL3)	555/70	52	10	23.5	141
	650/60	47			
	815/90	31.5			
	1625/150	7.5			

The sensors on-board R2A have been calibrated in laboratory for 100% albedo. In absence of an on-board calibration system and the inadequacy of single post-launch calibration methodology to fully calibrate the sensor, an integrated calibration approach was employed in the at-sensor radiance calibration of R2AL3 comprising of input from Laboratory calibration, moon image including the deep space region and cross calibration with contemporary sensor.

Laboratory Calibration

The LTC involves illuminating the detector elements with predetermined radiation intensity and recording the response of each element. The schematic representation of data acquisition during LTC is shown in Figure 2.

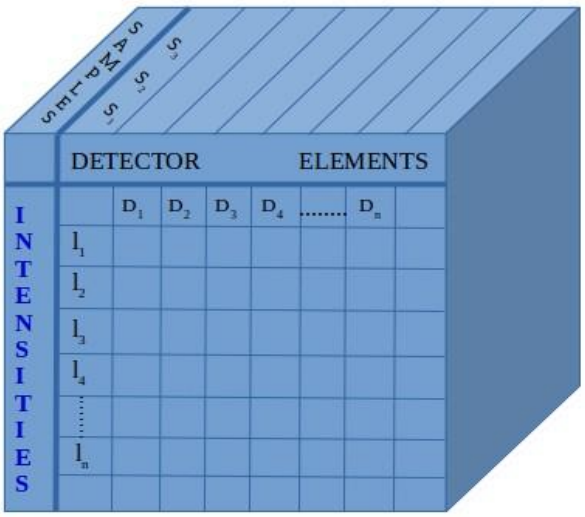

Figure 2 Data Collection during LTC

Large number of samples are then analysed at each intensity level in terms of a) sample-mean count for each element (pixel) of a sensor w.r.t radiance level to study the linearity of response and b) standard deviation of each pixel of a sensor w.r.t pixel mean count for the non-uniformity. The PRNU correction normalizes the response of all detector elements to the response of weakest element (one which generates maximum counts) for a given intensity. The post-correction response shows up in the form of lessened spread across the detector elements.

The variation in the response of detector-element to the input intensity in the form of Coefficient of Variation (CV) is compared with the PRNU-corrected response (Figure 3). It shows that the variation in counts after PRNU correction across the array for any given intensity is nearly eliminated.

After removing the differences in response of individual element, the linearity of response to input energy is characterized.

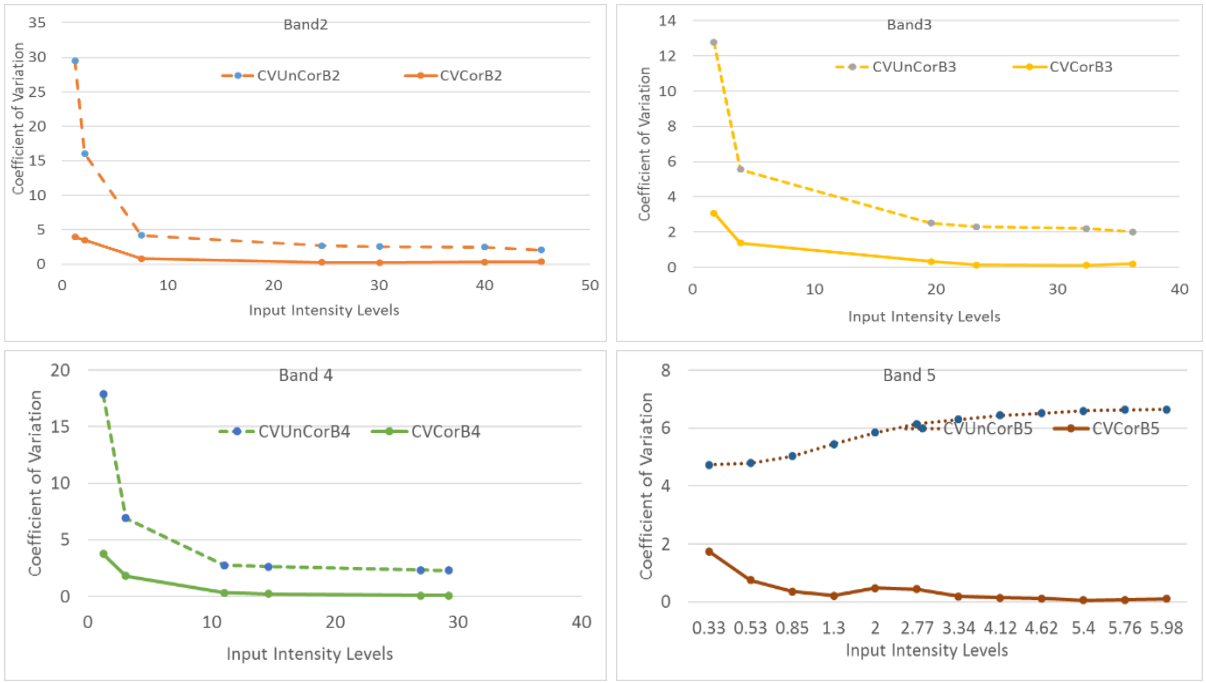

Figure 3 Comparison of CV before and after PRNU correction

The relationship between the input intensity and sensor response is essentially linear for most part of the input intensity. However, in the lower intensity region, the sensor shows a non-linear behaviour (see inset in Figure 4). Conventionally, the linear calibration coefficients are computed for the significant range without the elaborate dark current characterization, which leaves a negative offset.

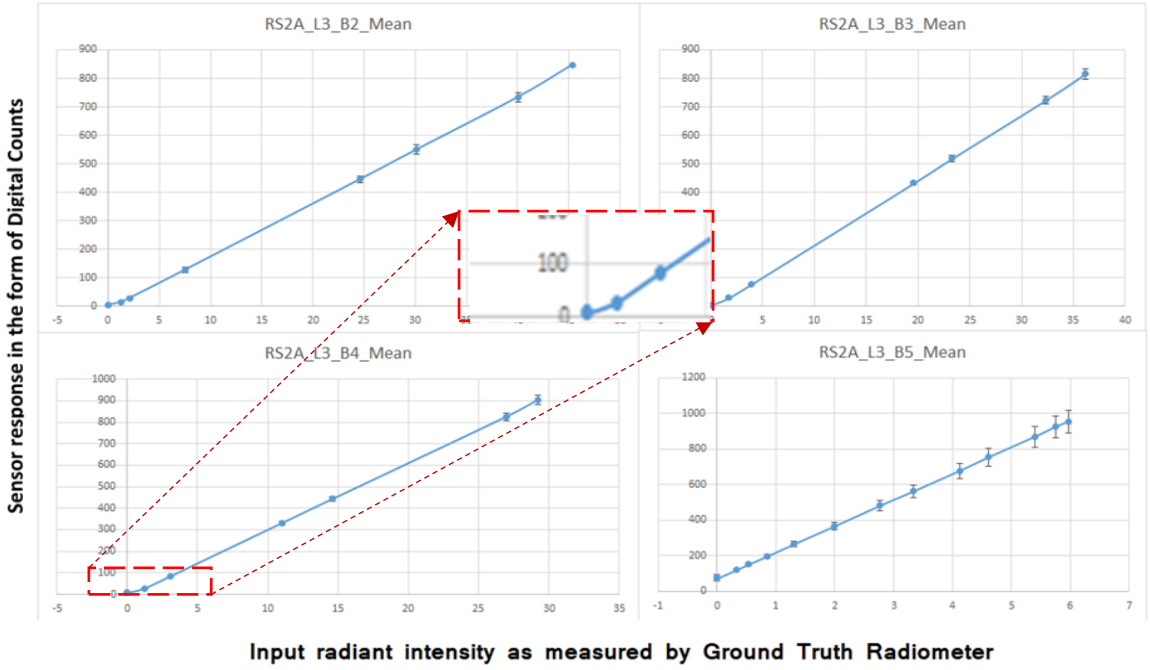

Figure 4 Sensor response to input intensity

Lunar calibration

The moon was acquired by R2AL3 sensor on 12Jan2017 to cover three segments of the device array. The information on lunar phase angle, time of acquisition and position of moon on device array is given in Table 2

Table 2 Moon position, phase and time of acquisition			
Position Name	Relative Position	Phase Angle (Source: GIRO)	Time of acquisition
A	Left	5.503	17:42:06.04
B	Centre	5.256	17:36:28.76
C	Right	4.872	17:29:40.08

The relative location of moon centre in terms of pixel number covered is shown in Figure 5.

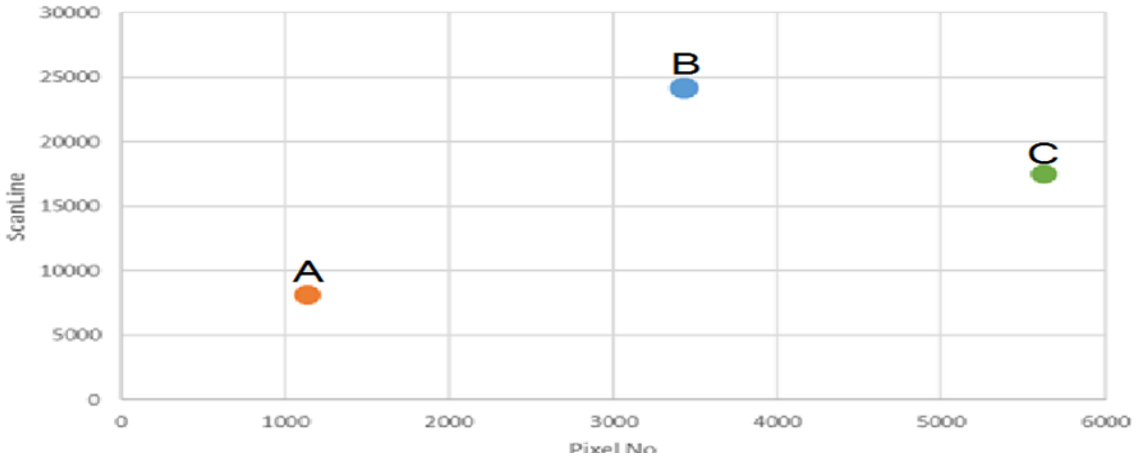

Figure 5 Position of moon centre on R2AL3 device

The deep space region surrounding the lunar image corresponds to zero-intensity dark region (MDC). The zero-intensity dark region from LTC data (LTCDC) and MDC for all bands across array are comparatively plotted in Figure 6

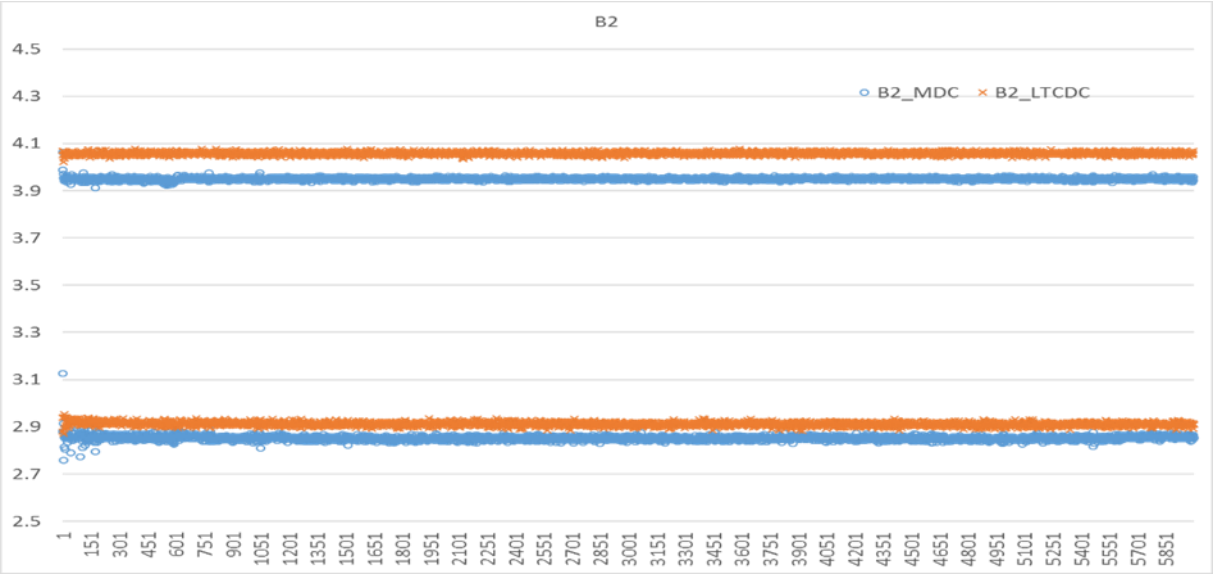

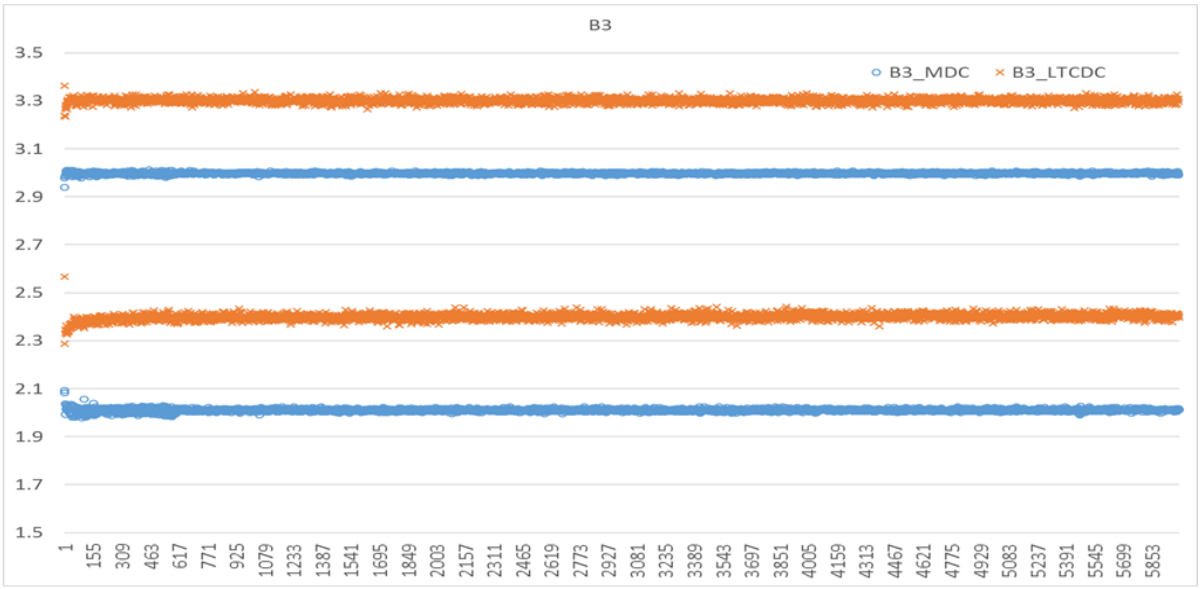

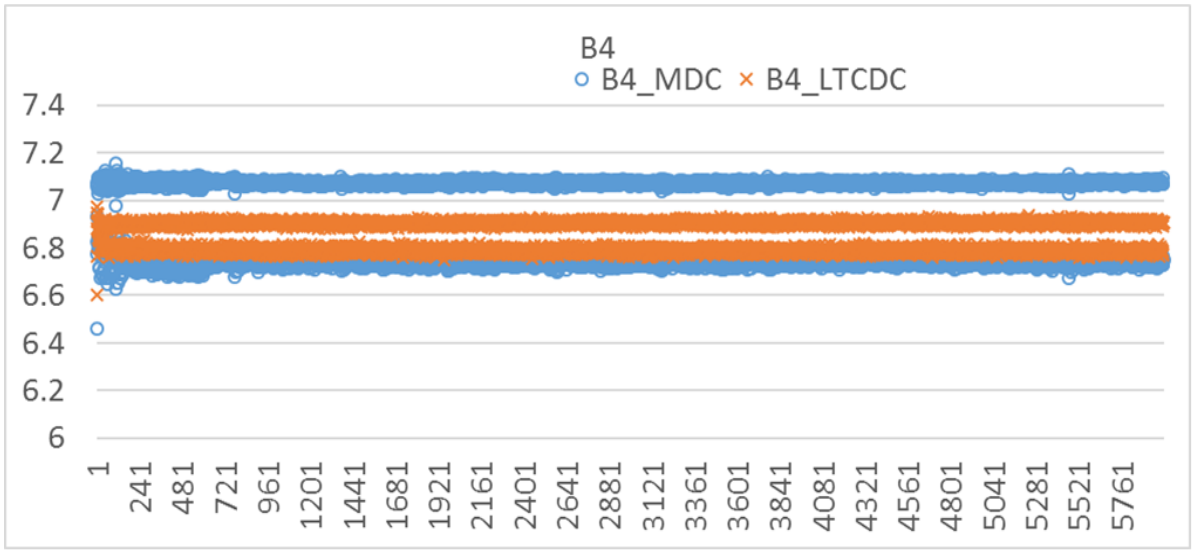

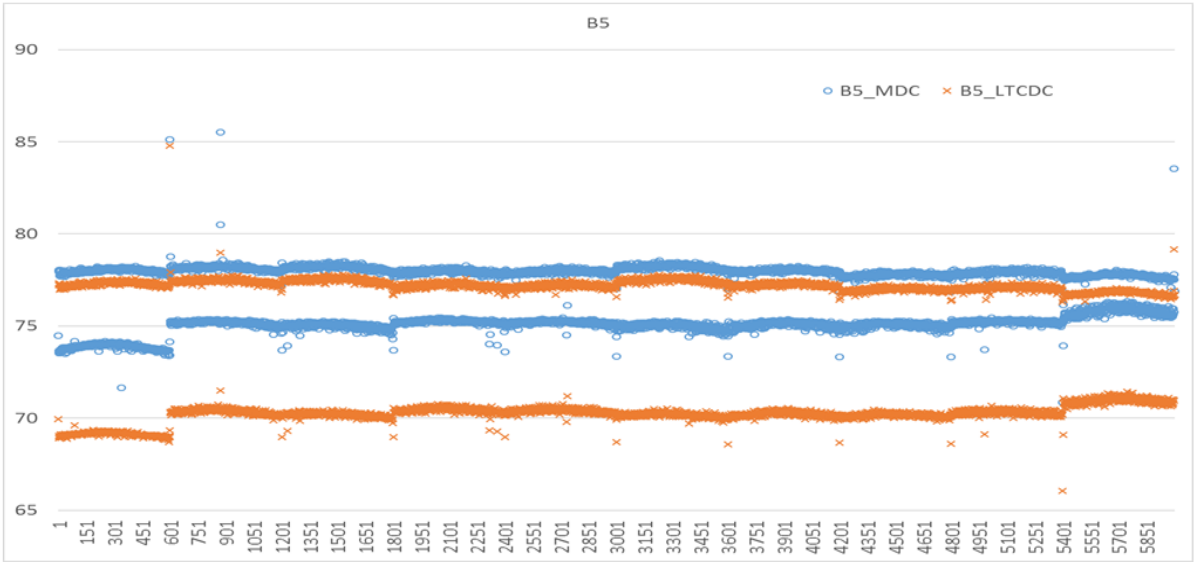

Figure 6 Comparison of dark count from laboratory (LTCDC) and from deep space (MDC). X-axis: Average Count; Y-axis: Pixel umber.

The DC versus pixel plot for two sources would have given two parallel lines if there was a bias between the two whereas Figure 6 shows four, nearly parallel lines. The pair of lines originating from single source of DC are due to the differences in odd and even detector element of the array. The symbols of the plot are explained in Table 3

Table 3 Explanation of legends in comparison plot

Symbol	Position	Represents	Detector Element
x	top	LTC DC	Odd numbered
o	top	Deep space DC	Odd numbered
x	Bottom	LTC DC	Even numbered
o	Bottom	Deep space DC	Even numbered

The dark current from LTC data for Band2 and Band3 is higher than DC obtained from deep space surrounding the moon. Although the magnitude of difference is varying. The summary of observations from Figure 6 is given in Table 4

Table 4Summary of Observations from Dark Current plot

Band No	LTCDC and MDC	Remarks
2	LTCDC>MDC	For even and odd
3	LTCDC>MDC	For even and odd; Larger difference
4	MDC>LTCDC	For odd only
5	MDC>LTCDC	For even and Odd; Difference is larger in even pixels

The integrated intensity of lunar surface has been reported to be stable over time. However, the spread in the intensity over the surface can be acknowledged seeing the histogram given in Figure 7.

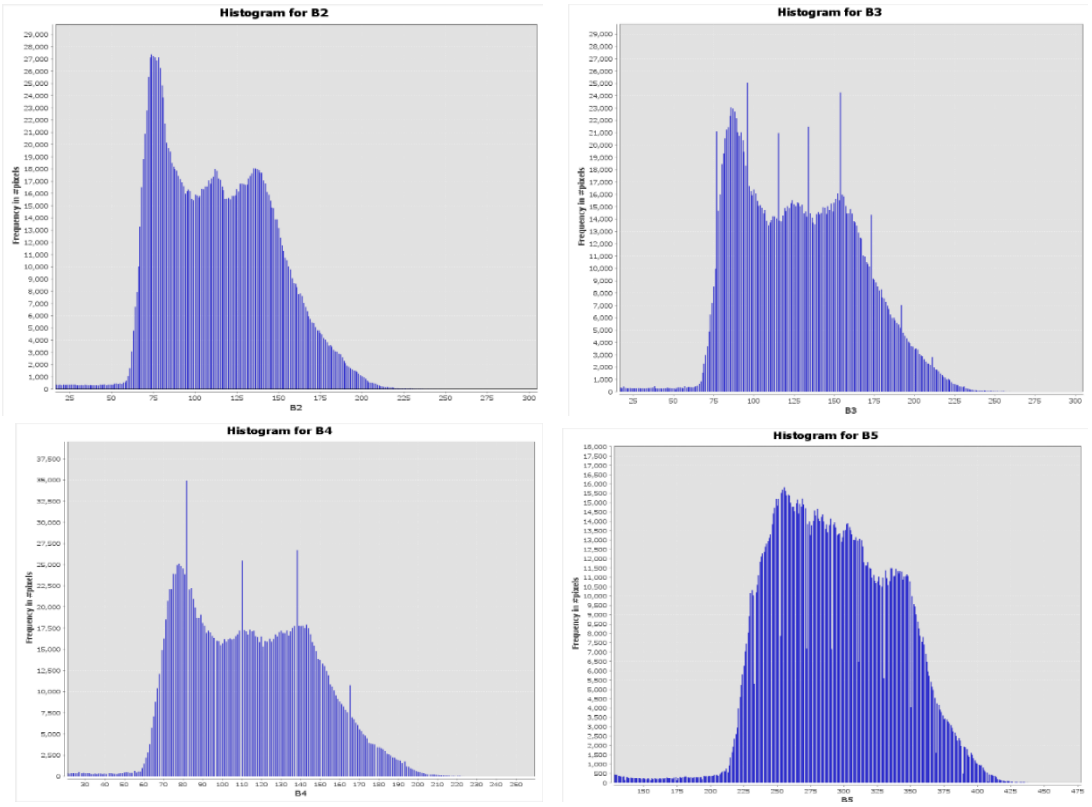

Figure 7 Histogram showing the range of counts covered by moon in L3 sensor

The spread in counts over the lunar surface is given in Table 5.

Table 5 The range of counts covered by moon in each of the R2AL3 bands		
Band No	Minimum Count	Maximum count
2	55	210
3	60	240
4	55	210
5	200	425

The use of moon as calibration source is limited to the disc-integrated irradiance, which is the aggregate of diverse intensity reflecting from lunar surface and the sensor's response to various intensity levels gets conglomerated.

In an attempt to harmonize the use of lunar irradiance reference generated by ROLO (EUMETSAT, 2014) and with an understanding to making same transfer function in context of instrument inter-calibration, the **G**SICS **I**mplementation of **RO**LO (GIRO) was developed and made available primarily to GSICS and CEOS IVOS member organizations.

The comparison between the reference lunar irradiance (I_{ROLO}) and the one observed by the sensor (I_{OBS}) is given in terms of **P**ercentage **D**is-**A**greement (PDA), given as:

$$PDA=(I_{ROLO}-I_{OBS}) *100/I_{ROLO}$$

The PDA for R2AL3 sensor is given in Figure 8

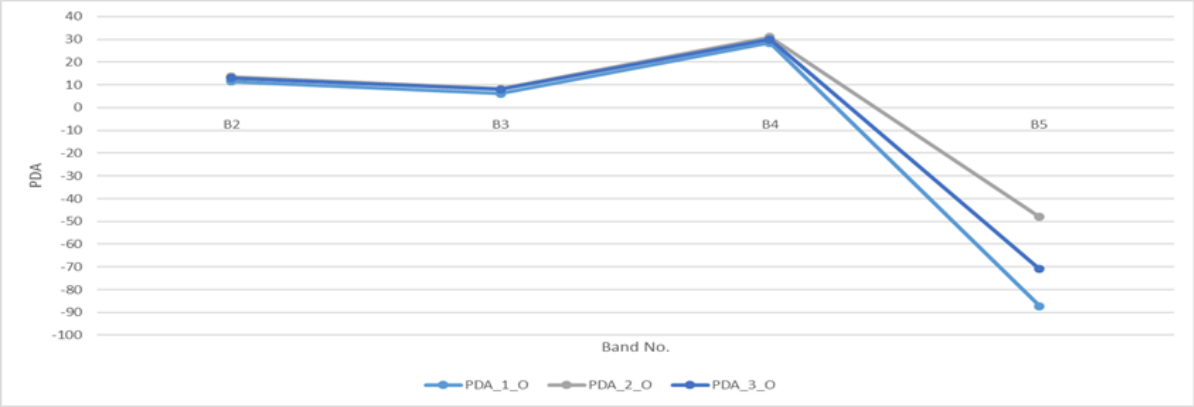

Figure 8 Percentage Disagreement between Observed and ROLO Lunar Irradiance for three acquisitions by R2A L3

The negative value of PDA points to ($I_{ROLO}<I_{OBS}$) condition and vice versa. It is evident from Figure 8 that for all bands except Band5, the observed lunar irradiance is lower by about 10% for B2, 7% for B3 and 30% for B4. The observed irradiance for B5 is higher by 50%-90% than the expected.

Cross Calibration

The cross calibration of a sensor with an identical sensor has been found to be cost-effective in terms of resources and time. The spectral bands of R2AL3 (Table 1) and its spatial resolution agrees closely to its contemporary sensor OLI on-board Landsat-8 (L8OLI). The spectral response function (SRF), also termed as Relative Spectral Response (RSR) is shown in Figure 9.

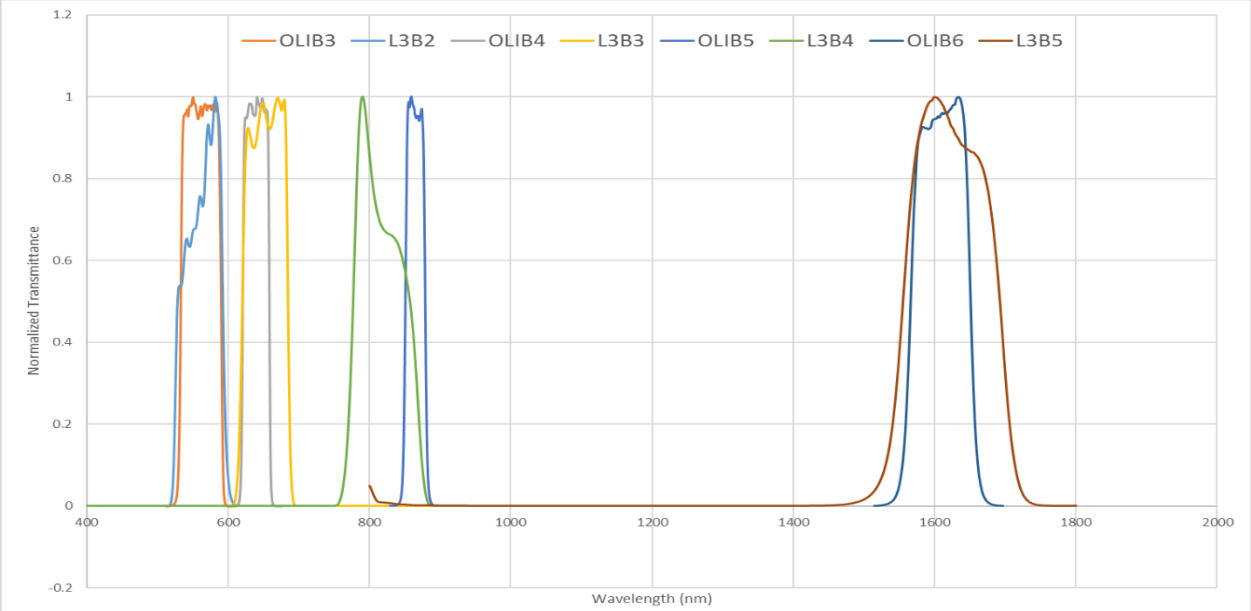

Figure 9 Relative Spectral Response of corresponding bands of R2AL3 and L8OLI

The proximity of spectral bands B3, B4, B5 and B6 of L8OLI is with B2, B3, B4 and B5 of R2AL3 respectively as can be seen from the figure where all bands, except L8OLIB5 and R2A-L3 B4, show large overlap with near coincident peak. In addition to the spatial resolution of L8OLI (30m) and R2AL3 (24m), the L8OLI has a repeat cycle of 16 days whereas R2AL3 revisits every 24 days. This creates a possibility of cyclic coincidence every 48 days. The WRS path 149 of L8OLI was found to coincide with Path 92 of R2AL3 on 20Dec2016 and again on 6Feb2017 as is shown in Figure 10.

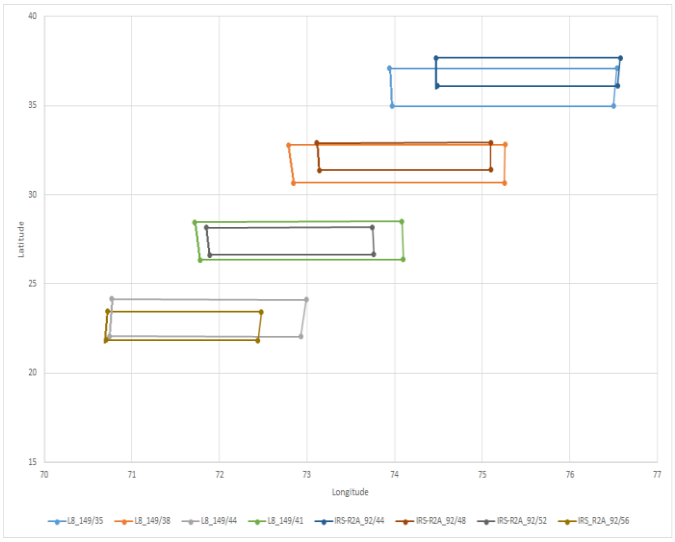

Figure 10 Coinciding regions of L8OLI and R2AL3

Additionally, the Path 92 Row 51 of R2AL3 covers the Bap calibration site which is used for carrying out vicarious calibration of ISRO's optical sensors (Shailesh Parihar, 2016). This also creates an opportunity to validate the calibration through surface reflectance products.

The calibration requires characterization of sensor's response to large range of incident energy; this implies that the cross calibration requires data acquired over ground features with bright through dark targets. The four data sets used for cross calibration during this exercise are shown in Figure 11.

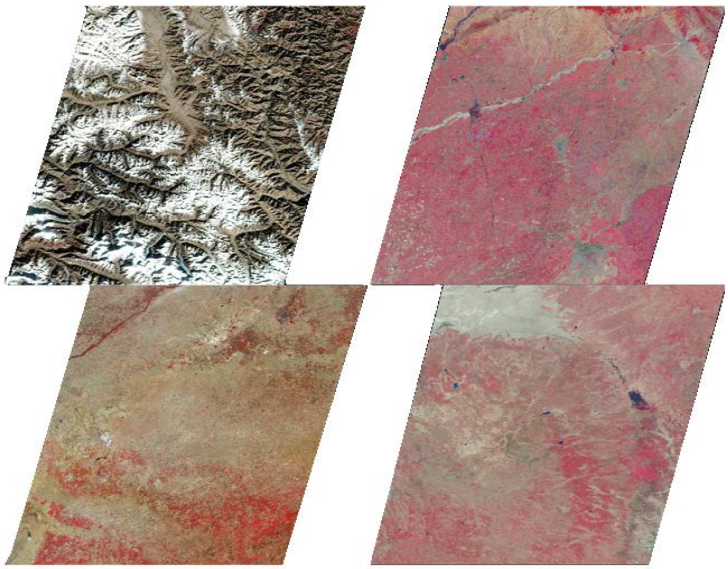

Figure 11 R2AL3 images covering various ground features

The scene centre time of data acquired by R2AL3 and L8OLI differs by approximately 20 minutes as can be seen from Table 6 which corresponds to a sun elevation angle difference of 1-2 degrees.

Table 6 Scene-centre time from data products of R2AL3 and L8OLI

Sr. No.	UTC Time (hh:mm:ss)		
	Scene centre		Difference
	R2AL3	L8OLI	
1	5:55:43	5:35:23	00:20:20
2	5:57:04	5:36:35	00:20:29
3	5:58:25	5:37:47	00:20:38
4	5:59:46	5:38:58	00:20:48

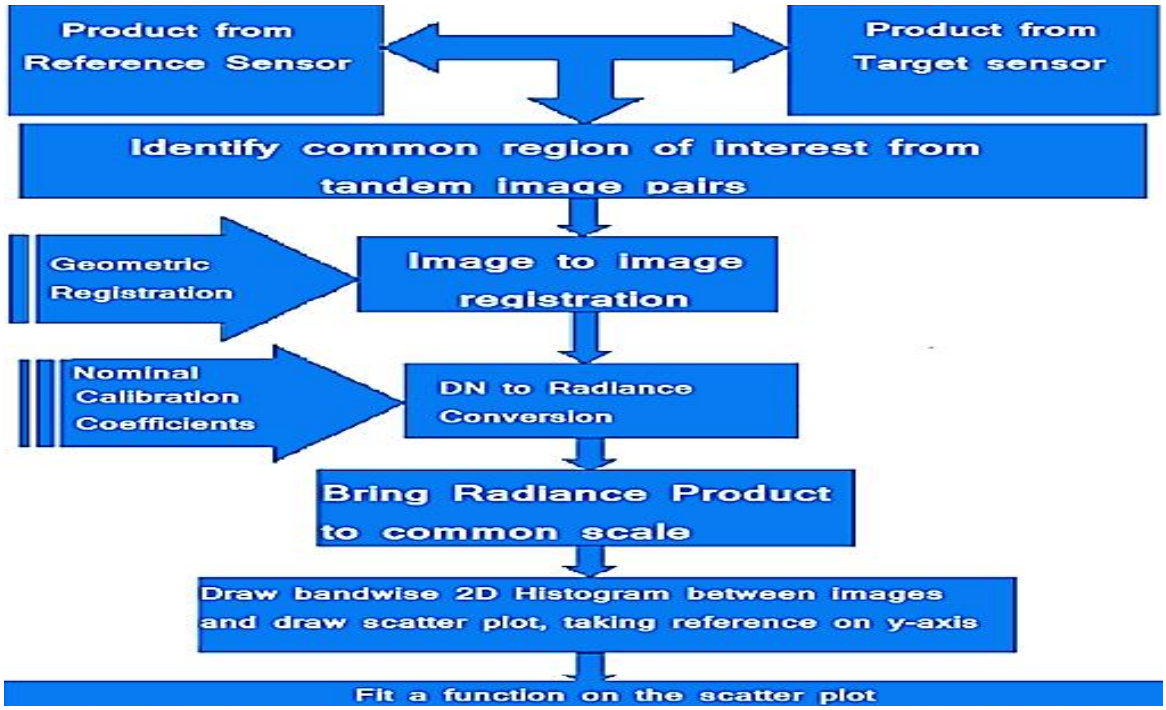

Figure 12 Flow chart showing the steps involved in cross calibration process

In addition to identifying co-located data which is imaged by the sensors that are being cross calibrated, the process requires to perform spatial as well as geometric registration so as to create a pixel-to-pixel correspondence between commonly available region of data-pairs. The steps involved in cross calibration process are given as a flowchart in Figure 12.

The histogram of corresponding data-pairs is computed and a scatterplot of modal frequency is plotted (Figure 13: The origin is at top left corner)

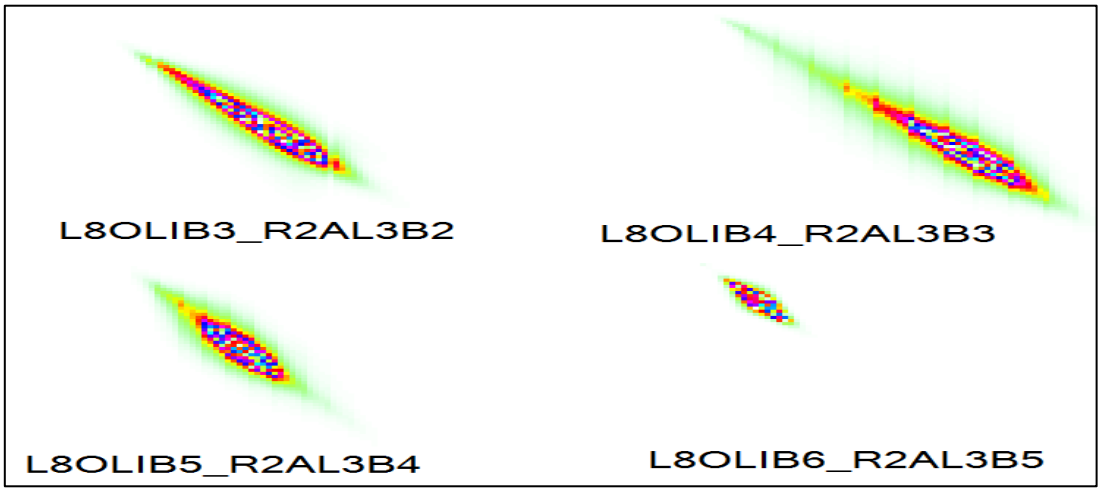

Figure 13 Scatter plot from 2D Histogram

An aggregate scatterplot from modal value of 2-D histogram is plotted with R2AL3 on x-axis and L8OLI on y-axis (Figure 14).

The scatterplot expresses various aspects of cross-relationship in the response of each sensor. The intersection of lines for various bands with the unit-line shows that the response of sensor is diametric in lower and higher intensities. It also shows a band-dependence in the cross-over position. The response is linear in the significant range of the histogram but in the dark intensity region it is non-linear, as was observed in LTC data. Outliers resulting from spatially and geometrically un-correlated points.

A function, which delineates the trend and circumvents the outliers, is fitted over the scatter plot for each band-pairs. Based on the trend in the scatter plot, a piece-wise coefficients have been fitted with a linear fit in the significant region of histogram whereas a non-linear (essentially, a quadratic fit) in the lower count values. The coefficients of the fitted function correlate the target sensor response to reference sensor response and hence, are the required calibration transfer functions.

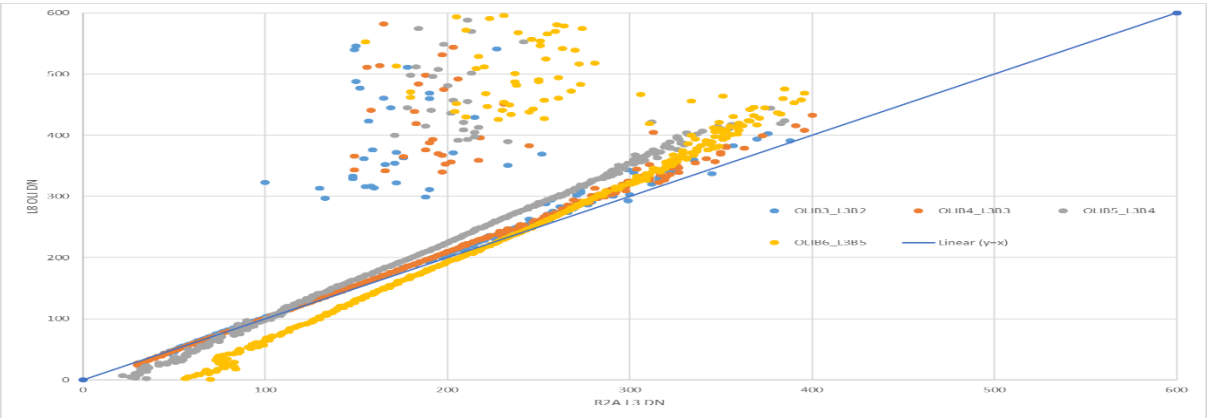

Figure 14 Aggregate scatter plot of Modal 2D histogram

Validation

The coefficients, thus derived, are validated by applying on moon data as well as sensor measured earth features. The PDA, which is a measure of closeness between measured and modelled lunar irradiance values, is compared between pre and post corrected lunar image (Figure 15).

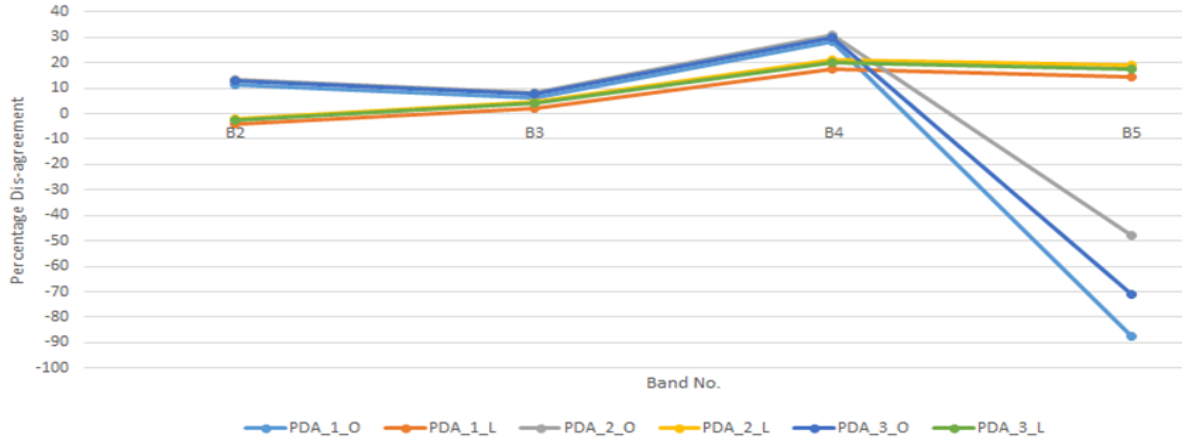

Figure 15 Comparison of PDA between Pre and Post Corrected Lunar data. 1, 2, 3 are acquisition session no.; O represents original data and L represent post correction data.

The PDA on lunar data after applying coefficients show improvement in two ways i) The large variation in PDA of band-5 in three acquisitions has been reduced to the extent of elimination and ii) the PDA, which was as high as 90%, has come down to less than 10% for B2, nearly zero for B3, under 20% for B4 and B5. The spectral signature of various features from the cross calibrated sensors are also compared.

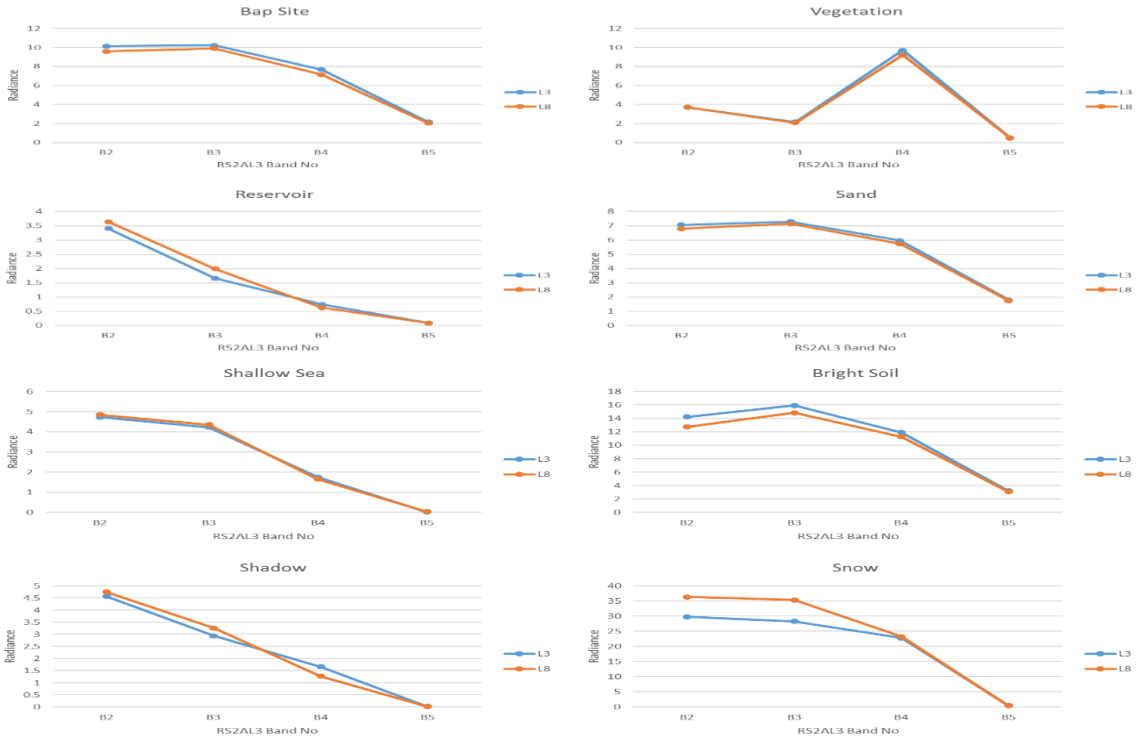

Figure 16 Comparison of at-sensor radiance signatures of various features

The R2AL3 data was re-processed using the cross calibration coefficients. The ground features have been chosen (Figure 16) so as to cover large part of sensor's dynamic range. The principal cause of the

minor deviations observed can be the difference in time of observation and feature reflectance property.

The validation of coefficients was also carried out through vicarious calibration method wherein four field campaigns were organized to cover target of different brightness level. Using synchronous surface reflectance and atmospheric measurements in the Second Simulation of Sensor Signal in Solar Spectrum (6S), modelled target radiances at the top-of-the-Atmosphere (TOA) was computed and compared (Figure 17) with the sensor measured radiance from non-calibrated data (Old) and data reprocessed using calibration coefficients (New).

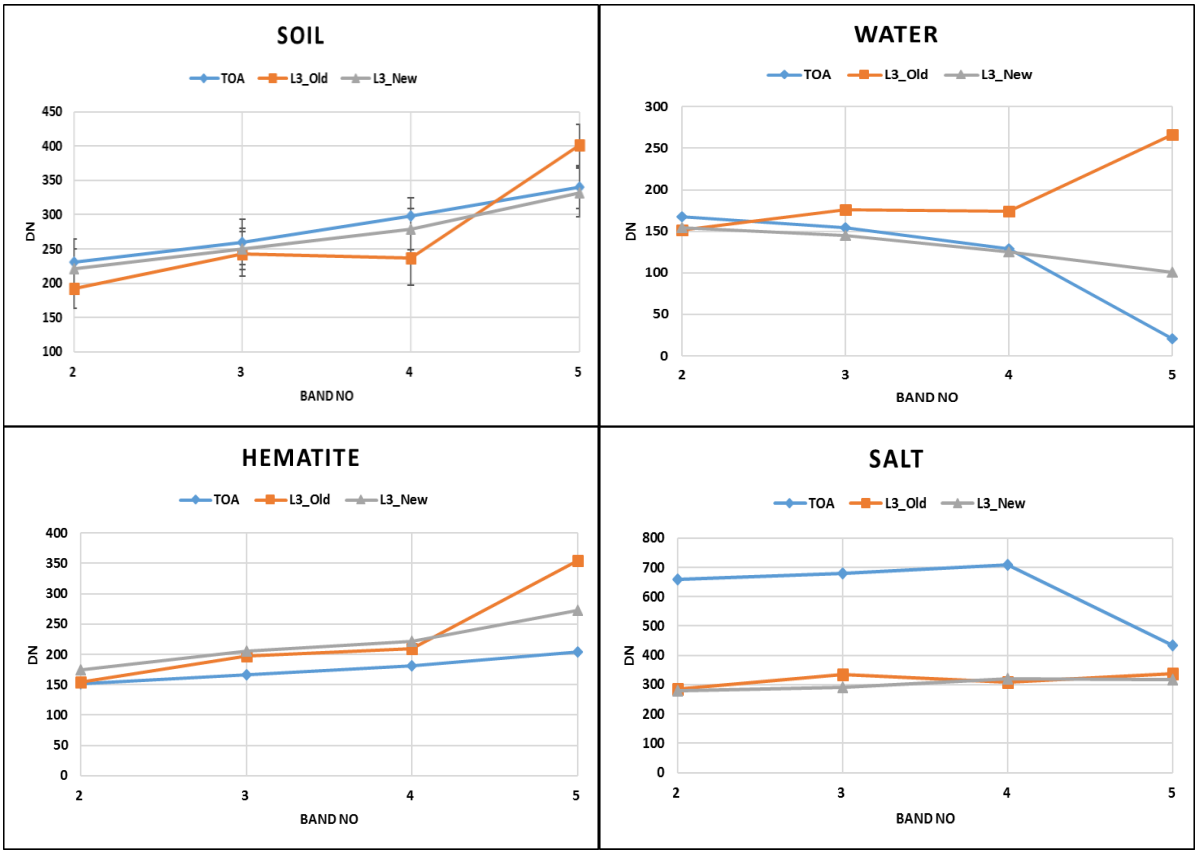

Figure 17 Comparison of TOA, L3(Old) and L3(New) Radiance for various features

Conclusion

The radiometric calibration of a sensor, which begins in the pre-launch stage through laboratory calibration, continues throughout the life of the mission in the post-launch stage. Unlike the pre-launch calibration, there are various methods to monitor the radiometric performance of the sensor. The uncertainty in determining the true dark current and limited intensity levels in laboratory calibration calls for additional methods for calibration. Although the Moon, with dark deep space background, fills the void of true dark current characterization, it is inadequate to span the full dynamic range of sensor. This can be achieved through cross calibrating the target sensor with respect to a reference sensor, whose radiometric calibration is known with certain confidence.

A generic approach of radiometric calibration was employed for R2AL3 sensor. It began with making a look-up-table from laboratory excluding the dark current and subsequently modified using dark current from deep-space of lunar data. To cover full dynamic range of the sensor, cross calibration against L8OLI was carried out using data of near-coincident pass. This resulted in non-linear calibration transfer coefficients, especially for dark region. These coefficients were applied on R2AL3 products and lunar imagery for validation. The PDA between measured lunar irradiance and modelled irradiance reduced to a large extent: reducing to <10% for band2, nearly zero for band3 and within <20% for band 4 and band5. The validation in the form of comparison of spectral signatures for various features from re-processed-R2AL3 and L8OLI also showed close match.

References

Desai, Y. P., Bhavsar, V. R., & Kartikeyan, B. (2011). *Calibration of OCM2 using Lunar Images and Comparison with ROLO.* Ahmedabad: IAQD/SIPG/SAC.

Eplee RE, B. R. (2004). SeaWiFS Lunar Calibration Methodology after Six Years on Orbit. *Proceedings of SPIE*, 1-13.

EUMETSAT. (2014). *Lunar Calibration Workshop Background and Agenda.* EUMETSAT.

IAQD Calval Team. (2017). *RADIOMETRIC AND SPATIAL CHARACTERIZATION OF SENSORS ON-BOARD CARTOSAT-2D USING ARTIFICIAL TARGETS.* Ahmedabad: IAQD/SIPG/SAC.

RESOURCESAT-2 DQE Team. (2010). *RESOURCESAT-2 Data Quality Evaluation Software Requirements Specification, Architecture & Detailed Design.* Ahmedabad: IAQD/SIPG/SAC.

Ron Morfitt , Julia Barsi , Raviv Levy , Brian Markham , Esad Micijevic ,Lawrence Ong , Pat Scaramuzza and Kelly Vanderwerff. (2015). Landsat-8 Operational Land Imager (OLI) Radiometric Performance On-Orbit. *Remote Sensing*, 2208-2237.

Shailesh Parihar, L. R. (2016). ite Characterization for Calibration of Radiometric Sensors using Vicarious Method. *SPIE*, 1-6.

Stone, T., & Kieffer, H. (2007, July 17-19). Lunar Calibration: Using the Moon as a Calibration Source for Earth-Observing Instruments in Orbit.

Teillet P M, M. B. (2006). Landsat cross-calibration based on near simultaneous imaging of common ground targets. *Remote Sensing of Environment*, 264-270.